Appl. Phys. B 63, 575–583 (1996)

Applied Physics B Lasers and Optics

Influence of the electric field frequency on the performance of a RF excited CO_2 waveguide laser

V. N. Ochkin[2], W. J. Witteman[1], B. I. Ilukhin[2], I. V. Kochetov[2] P. J. M. Peters[2], Yu. B. Udalov[1], S. N. Tskhai[1]

[1] Department of Applied Physics, University of Twente, P.O. Box 217, 7500-AE Enschede, The Netherlands
(Fax: + 31-534843965, E-mail: udv@UTEP.ELTN.UTWENTE.NL)
[2] P.N. Lebedev Physics Institute, Russian Academy of Sciences, Leninsky Prospect 53, 117924, Moscow, Russia

Received: 11 December 1995/Accepted: 26 April 1996

Abstract. An analysis is presented of the effect of the RF frequency on the active media of CO_2 waveguide lasers. It is found that the characteristics are improved with increasing RF frequency because the space charge sheath width decreases with increasing excitation frequency. We also found that the sheath width decreases with the discharge current; this fact was never discussed before. The higher the exciting frequency the higher is the maximum input power of the discharge in the stable low current mode. It is attractive to extend the input power while keeping the discharge in this mode. Finally, a stabilizing excitation technique is described for the inherent unstable region of the discharge.

It is well known that the best performance of CO_2 waveguide lasers is obtained with RF excitation [1–6]. The choice of the used excitation frequency was mainly determined by practical arguments like the available power supplies. Its impact on the laser performance has not been studied thoroughly. So far this problem received little attention. There are two main points of view. There is the opinion that a change of frequency influences only the properties of the quasi-neutral plasma of the active medium [2, 7]. The other one is that the frequency changes the thickness of the charge sheaths near the electrodes so that the energy deposition into the quasi-neutral plasma and consequently the laser output are influenced [8, 9]. The theoretical background for these considerations was discussed either phenomenologically or qualitatively.

In a previous paper we presented the laser characteristics of the CO_2 waveguide system with RF discharge [5]. The present paper, based on the previous model, will analyse the mechanism of laser excitation as it depends on various parameters, especially on the RF field frequency.

1 Initial assumptions and system description

The system that will be analysed theoretically is our experimental device [4, 5] having a waveguide discharge volume of $2.25 \times 2.25 \times 370\ mm^3$. The used gas mixture is CO_2–N_2–He (1:1:8) at a pressure of 100 Torr. The RF voltage is by means of parallel shunt inductors homogeneously applied to the two parallel electrodes. The field distribution in the discharge is calculated by solving the Poisson equation with the appropriate boundary conditions determined by the oscillating voltage over the electrodes. Because of the homogeneity of the RF discharge the problem is treated one-dimensionally with the coordinate x perpendicular to the electrode surfaces. The Boltzmann equation for the electron energy distribution is then solved by using the relevant cross-sections for the electronic excitations, vibrational excitations, dissociation of the CO_2 molecule and the ionisations of N_2 and CO_2. The discharge heat is removed through both electrodes and through the ceramic side walls of the cavity. The considered frequencies of the electric field are in the range from 62 to 233 MHz. The relaxation frequency of the electron drift velocity is assumed to be larger than the frequency of the electric field. This condition limits the field frequency.

Due to the time dependent plasma formation of the discharge, the discharge current is not in phase with the externally applied voltage. The current is not even harmonic. For that reason the Fourier analysis is applied to calculate the relevant parameters like impedance and energy deposition. The effects of the dissociation products, carbon monoxide and oxygen, on the discharge are also taken into account.

The laser field is described by the fundamental waveguide mode EH_{11}. The cavity losses are described by a distributed loss $\alpha = 10^{-4}\ cm^{-1}$ and the outcoupling through one mirror is obtained by a transmission $T = 5\%$, while the other mirror is considered as a 100% reflector. The variable parameters are the frequency and the input RF power. A more detailed description of the present model and its justification are given in [5].

2 The effect of the space charge on the laser process

With the method described in [5] we calculated numerically the laser parameter values for three discharge frequencies which are 62, 125 and 223 MHz. At first, all calculations are performed for 200 W input power. The results are shown in Table 1. The voltage amplitudes over the electrodes show a significant frequency dependence for constant input power. It is seen that the reduced electric field strength (E/N) in the quasi-neutral central plasma (the root-mean-square, RMS value) is not sensitive to the discharge frequency. Its value is near the optimum value for the excitation of the upper level. Both the gas temperature and the discharge current change slowly with frequency. In contrast to that, the electric field and the structure of the discharge impedance change significantly. Since the impedance of the discharge due to plasma formation kinetics is nonlinear with the applied voltage it is found that the current deviates from the harmonic oscillation and its first Fourier harmonic has a phase delay with respect to the applied harmonic field. In Table 1 the cosine of this phase delay is indicated. The variations of the discharge properties are caused by specific processes near the electrode layers where the plasma properties are far from optimal for lasing.

Table 1.

Frequency [MHz]	62	125	223
Voltage amplitude	324	202	167
Modulus [Ω] of discharge impedance	129	72.1	56.9
Cosine of the angle between the first current harmonic and the voltage to the electrodes	0.508	0.719	0.828
Active resistance R_s [Ω]	65.6	51.8	47.1
Reactive resistance X_s [Ω]	111	50.1	31.8
Full current amplitude I_m [A]	2.36	2.59	2.74
The first harmonic current [A] amplitude I_0	2.51	2.80	2.93
Difference between full current value and its first harmonic [%]	0.6	0.8	0.8
Reduced electric field in a quasi-neutral plasma E_{RMS}/N [V cm^2 10^{-16}]	1.86	1.99	1.99
Reduced electric field close to the electrodes E_{RMS}/N [V cm^2 10^{-16}]	33.2	21.7	14.7
Gas temperature at the centre of the discharge gap [K]	493	511	515

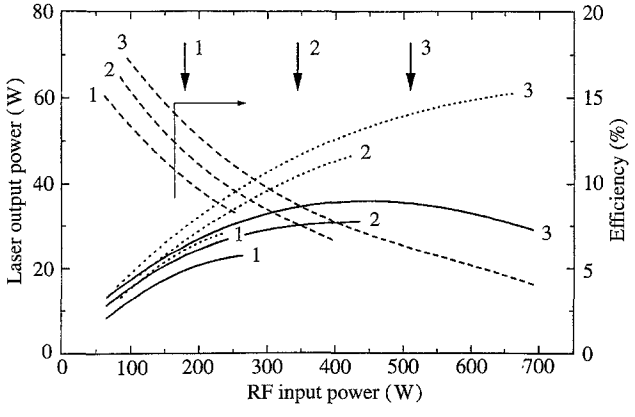

Fig. 1. The dependence of the laser output power (solid and dotted lines) and efficiencies (dashed lines) on the input power (1) $f = 62$ MHz, (2) $f = 125$ MHz, (3) $f = 223$ MHz. The dotted lines refer to mixtures without dissociation

Next we calculate according to the procedure indicated in [5] the laser power and conversion efficiency as they depend on the discharge frequency. This is done as a function of the input power. In Fig. 1 we plotted the output power (solid lines) and laser efficiency (dashed lines). We also plotted the laser output (dotted lines) in the case dissociation of the CO_2 molecules is left out. The numbers 1, 2 and 3 refer, respectively, to the frequencies 62, 125 and 223 MHz. The arrows with numbers pointing to certain input energies will be discussed later on in Sect. 4. It is seen that the output as a function of the input reaches a maximum that depends on the RF field frequency. The efficiency decreases with input power because of the increasing lower level population at elevated gas temperatures. The main result so far is the increased output power and efficiency with field frequency. This will be explained in the following.

In Fig. 2a the E/N value (RMS) and the gas temperature as a function of the distance from the centre of the discharge gap are plotted for the three field frequencies at a constant input power of 100 W. In Fig. 2b the corresponding local dissipated power densities are plotted. The power is mainly delivered by the electrons. However, near the electrodes the ion concentrations are considerable so that the fractional energy dissipated by the ions cannot be neglected. The dashed lines represent the power transfer to the electrons. In Fig. 2c the small signal gain (solid lines) and the saturated gain (dashed) are plotted. The dotted line represents the intensity distribution of the EH_{11} mode. It is seen that near the electrodes there is a remarkable change in the gain for the different frequencies. The gain depends on the power input (Fig. 2b), the gas temperature (Fig. 2a) and the E/N value that determines the effective vibrational excitation of the N_2 molecules by the electrons. In Fig. 2d we plotted the saturation intensity and the kinetic efficiency profile. The saturation intensity I_s is equal to $h\nu/\sigma_s\tau$, where σ_s is the cross-section of simulated emission and τ the lifetime of the upper laser level. It varies mainly in our situation with the vibrational lifetime of the upper laser level. Under our conditions the relaxation rate of the upper level depends much strongly on the gas temperature than on the decrease of the density with increasing temperature in the centre. The kinetic efficiency is defined by

$$\eta(x) = \frac{G_0(x) I_s(x)}{W(x)} \tag{1}$$

where $G_0(x)$ is the (saturated) gain. $I(x)$ is the intra-cavity radiation intensity and $W(x)$ is the electric power density. In Figs. 3–5 similar results are plotted as in Fig. 2 for different input powers and field frequencies. Figure 3 gives the results for an electric field frequency of 62 MHz and an input power of 250 W. In Fig. 3a we plotted the reduced electric field (RMS) indicated by (1), the energy dissipation density (2), the energy dissipation by the electrons (2'), and

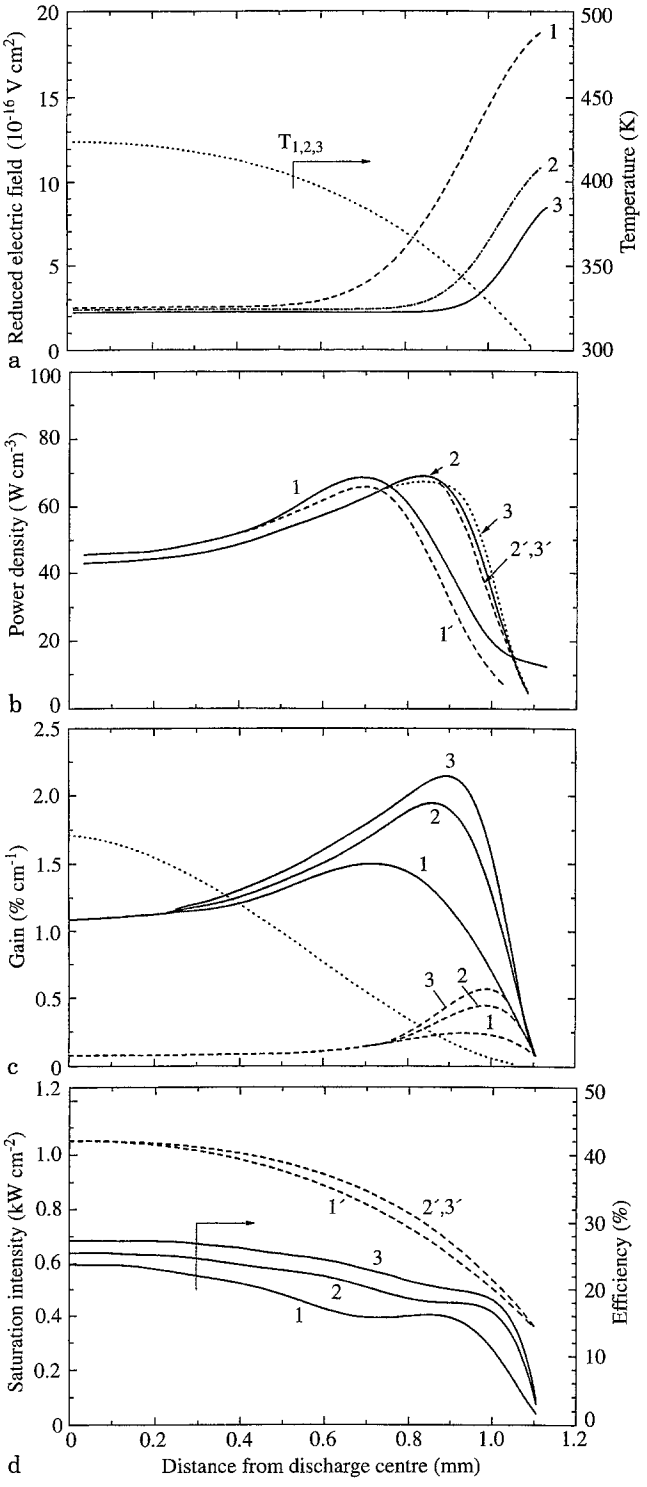

Fig. 2a–d. Spatial structure of the laser plasma parameters, averaged over the field period, for an input power of 100 W. (1) $f = 62$ MHz, (2) $f = 125$ MHz, (3) $f = 223$ MHz. (**a**) Root-mean-square of the reduced electric field strength and the temperature of the neutral gas. (**b**) Total input power density (1, 2, 3), and the input power density of the electrons (1′, 2′, 3′). (**c**) Small signal gain (solid lines) and saturated gain (dashed lines), and the spatial distribution of the emitted power in the fundamental waveguide mode EH_{11} (dotted line). (**d**) Kinetic efficiency (solid lines) and saturation intensity (dashed lines)

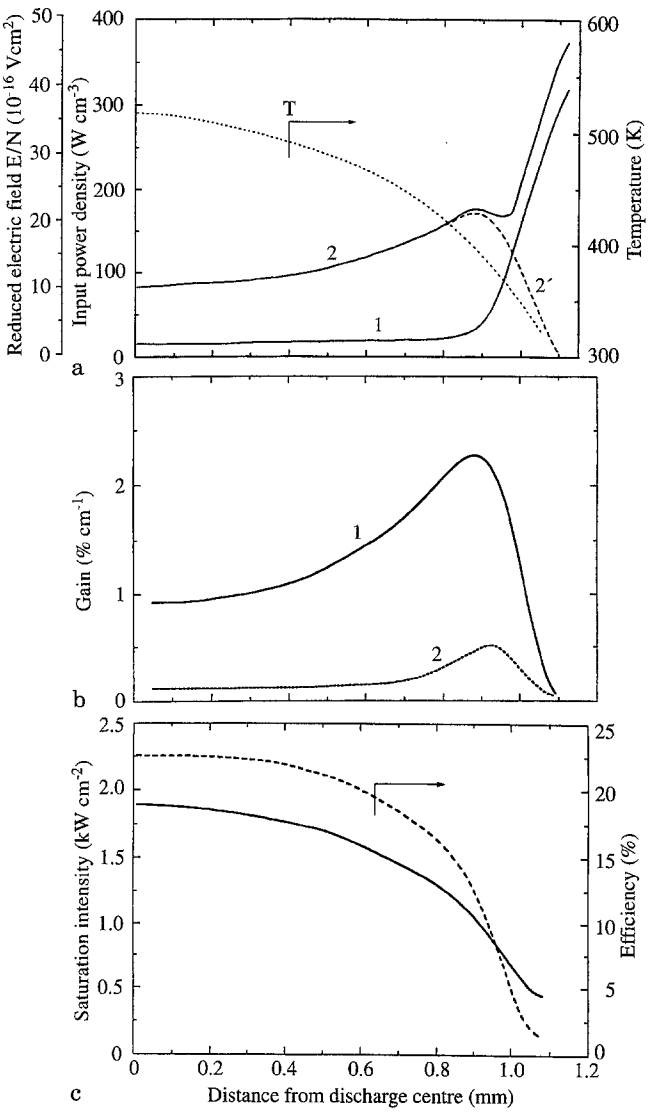

Fig. 3a–c. Parameters and profiles of the discharge and the laser at an input power of 250 W and a frequency of 62 MHz. The plotted data are averaged over the field period. (**a**) Root-mean-square of the reduced electric field strength (1), total input power density (2), input power density of electrons (2′), neutral gas temperature (T). (**b**) Small signal gain (1, solid line) and saturated gain (2, dashed line). (**c**) Kinetic efficiency (dashed line), and saturation intensity (solid line)

the gas temperature profile T. Figure 3b shows the small signal gain (1) and the saturated gain (2). Figure 3c shows the saturation intensity and the kinetic efficiency. In Figs. 4 and 5 the results are plotted for 125 MHz with 600 W input and 223 MHz with 700 W input power, respectively. We find that higher input powers and higher frequencies result in a decrease of the sheath width and also in a steeper increase of the parameter values near the electrodes. The decrease of the thickness of the space charge sheath improves the laser performance. We notice that the calculated results are obtained by assuming stable discharges. However, experimentally it is observed that the stability regime is restricted [1]. The theoretical background of a limited stability regime will be discussed in the following paragraph.

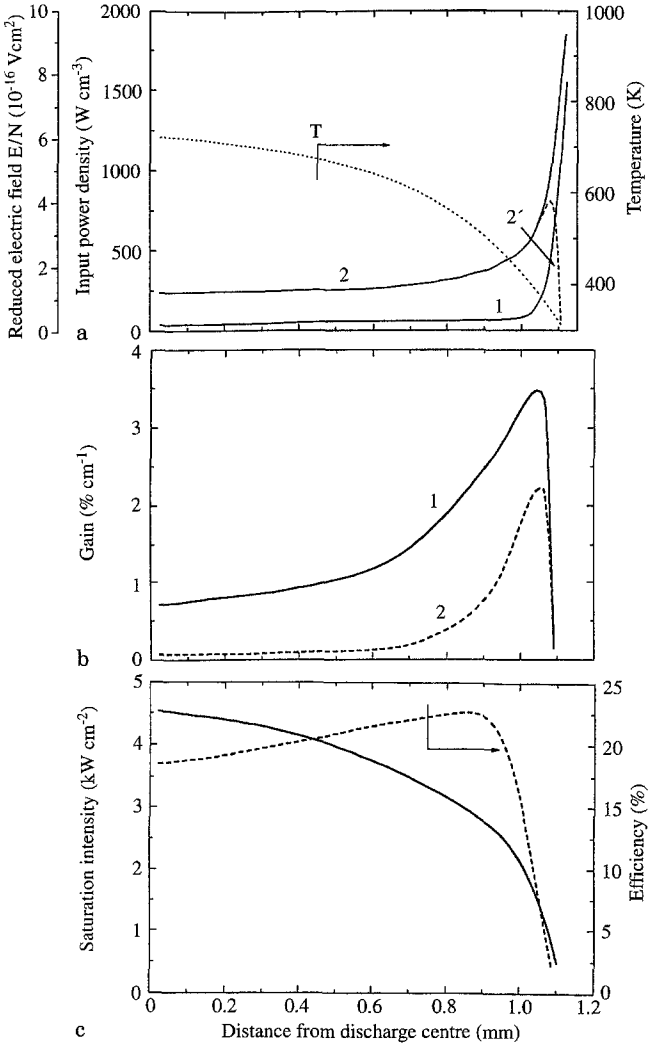

Fig. 4a–c. Parameters and profiles of the discharge and the laser at an input power of 600 W and a frequency of 125 MHz. The plotted data are averaged over the field period. **(a)** Root-mean-square of the reduced electric field strength (1), total input power density (2), input power density of the electrons (2′), neutral gas temperature (T). **(b)** Small signal gain (1, solid line) and saturated gain (2, dashed line). **(c)** Kinetic efficiency (dashed line), and saturation intensity (solid line)

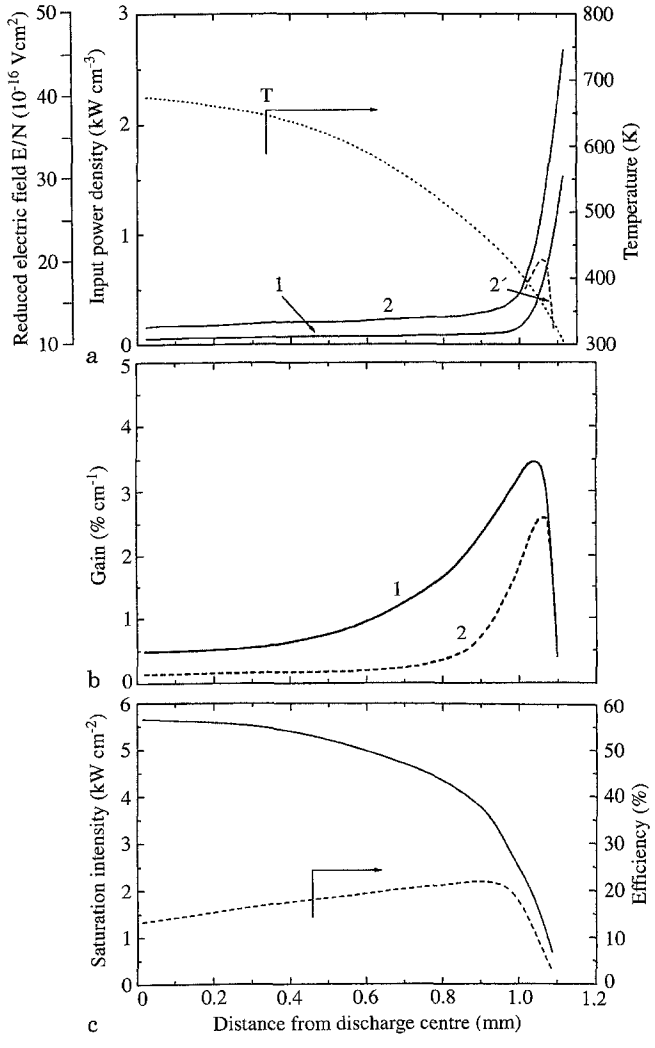

Fig. 5a–c. Parameters and profiles of the discharge and the laser at an input power of 700 W and a frequency of 223 MHz. The plotted data are averaged over the field period. **(a)** Root-mean-square of the reduced electric field strength (1), total input power density (2), input power density of the electrons (2′), neutral gas temperature (T). **(b)** Small signal gain (1, solid line) and saturated gain (2, dashed line). **(c)** Kinetic efficiency (dashed line), and saturation intensity (solid line)

3 Discharge characteristics and the stability regime

It is well known that the Voltage–current Characteristics (VIC) of direct current (DC) discharges have a negative slope i.e. these discharges are unstable. Circuit stability can then be obtained by inserting a ballast resistor in series. This introduces additional power losses and lowers the efficiency [1, 11]. An additional advantage of the RF discharge is the absence of a ballast resistor. From a theoretical point of view, it is not clear under what conditions this occurs; in particular one may wonder, in what range of energy deposition the stability is expected, and furthermore, how it depends on gas density and electric field frequency. First approximations to this problem were found in [8, 9]. In the following, we shall describe the discharge behaviour in much more detail. The present model of the discharge properties for RF excitation allows a study on the basic mechanisms of the VIC.

3.1 The voltage–current characteristics

The input power W into the discharge is given by:

$$W = \frac{S}{T}\int_0^T \mathrm{d}t \int_0^l j_c(x,t)E(x,t)\,\mathrm{d}x, \tag{2}$$

where S is the electrode area, j_c the conduction current density, E the electric field, l the distance between the electrodes and T the period of the electric field. Further, we calculate from our model the VIC curves. For the current and voltage we take the root-mean-square values.

In Fig. 6 the solid curve 1 (OABCD) is the VIC characteristic for 62 MHz. The curve 1′ (O′A′B′C′D′) presents the dependence of the voltage on the conduction current in the centre of the discharge. Comparing the two curves it is instructive to discuss some parts of these curves.

A. The part AO represents the characteristic without discharge breakdown. The current is simply displacement current I_d determined by the capacitance of the electrodes or $I_d = V\omega C$ where ω and C are the circular field frequency and the capacitance of the electrodes, respectively.

B. The point A on the part AB indicates the breakdown of the discharge. At low energy deposition (low conduction current) the charge density is small and the Debye radius is comparable to or higher than the electrode distance. In that case, a volume charge exists in the whole space between the electrodes. As the input power (conduction current) increases both the absolute values of electron and ion density including their difference increase too. In Fig. 7a we show the densities of electrons, n_e, of the difference between positive and negative ions $N = N^+ - N^-$ and of the difference between ion charges and electrons $q = N - n_e$. These quantities are plotted for two different input powers as indicated in the figure. The results in Fig. 7a refer to the AB part of the characteristics whereas Fig. 7b refer to the CD part of the characteristic. At the low energy depositions of Fig. 7a there is no sheath formation near the electrodes [10]. The electric field strength $\bar{E}(x)$ averaged over half a period is determined from the Poisson equation by taking also the time average

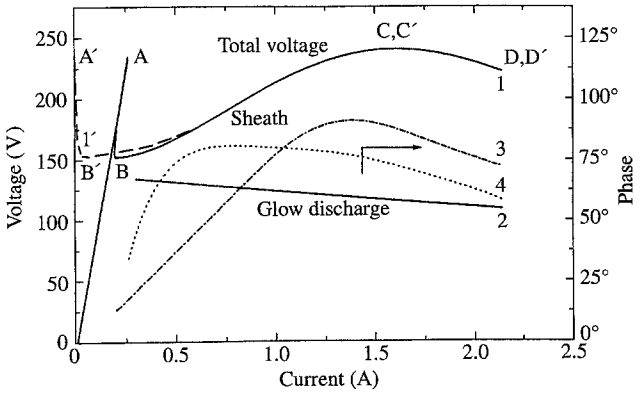

Fig. 6. Voltage–current characteristics (RMS values) of the discharge at the frequency of 62 MHz. (1) an (1′) are the dependence of the voltage to the electrodes and the voltage to the conductive current of the discharge on the total current and on the conductive current, respectively. (2) is the voltage–current characteristic of a positive glow discharge. (3) is the voltage–current characteristic of the sheaths near the electrodes. (4) is the dependence of the phase difference ϕ_{sp} between the sheath voltage and the plasma voltage as a function of total current.

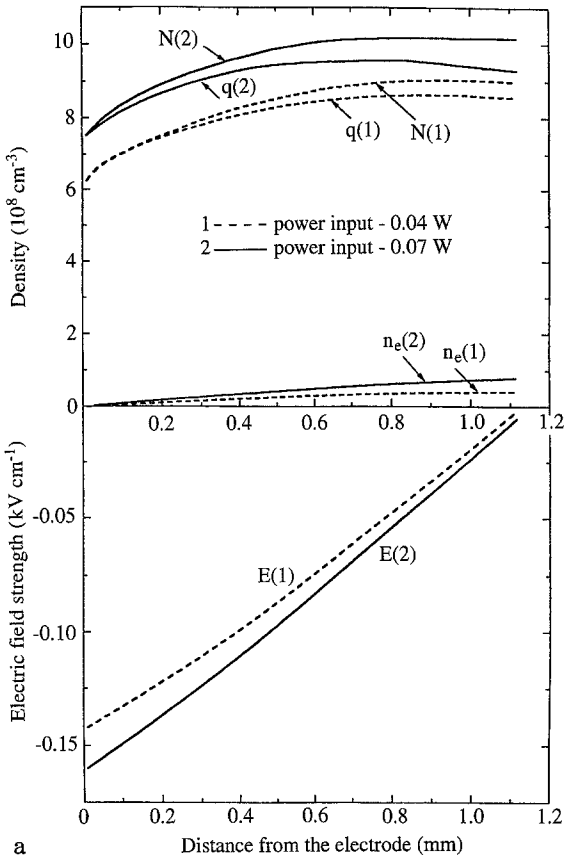

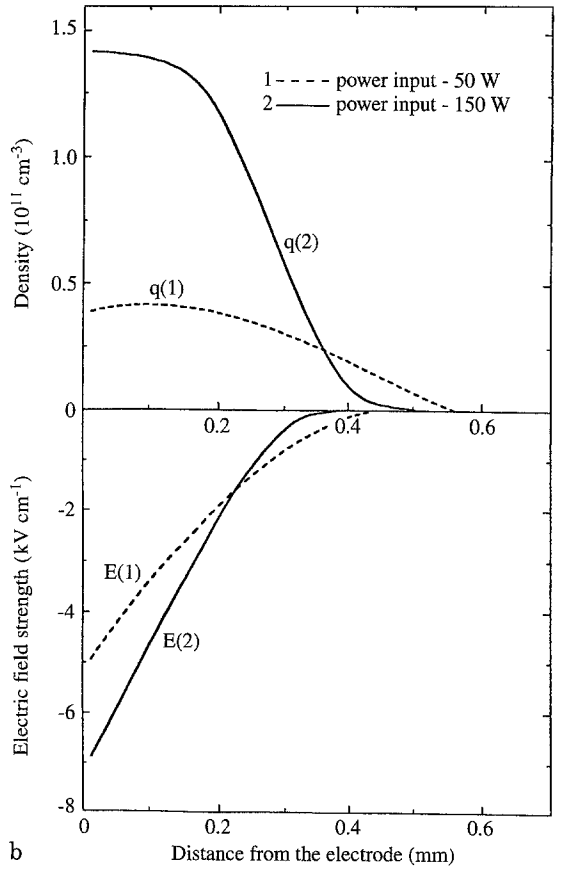

Fig. 7a, b. Charges and the time averaged electric field strength distributions at the frequency of 62 MHz. n_e is the electron density, $N = N^+ - N^-$ is the difference between positive and negative ion densities and $q = N - n_e$; **(a)** Low input power according to the AB part of Fig. 6. **(b)** Input power according to the CD part of Fig. 6

of the charge $\bar{q}$:

$$\bar{E}(x) = 4\pi e \int_0^x \bar{q}\,dx, \tag{3}$$

where the charge $\bar{q}$ includes also the charge layer attached to the electrode; x is the distance from the surface of an electrode. These values are also plotted in Fig. 7a. We notice the increase of electric field strength with power.

In the range AB, the displacement current exceeds substantially the conduction current. However, when the conduction current grows with increasing input power because of increasing ion density, the impedance of the discharge decreases and also the voltage U between the electrodes. This, on its turn has a decreasing effect on the displacement current which is proportional to U. The main variations of the discharge current occur in the region OAB of the characteristic.

C. In the region BCD the conductivity of the discharge increases with input power and the conduction current dominates. The displacement current at higher current is much smaller than the conduction current and the total current is in fact the conduction current. As the energy deposition increases, the sheath with the positive charge becomes stronger. This agrees with qualitative models [10, 12] and a theoretical prediction [11].

The typical spatial distribution of the charge density and the electric field strength are shown in Fig. 7b for input powers of 50 W and 150 W. Since the discharge characteristics in the centre with the quasi-stationary plasma discharge and near the electrode with the sheath formation strongly differ it is necessary to analyse separately the two parts of the VIC which refer, respectively, to the sheath and the plasma.

We use the following method. Firstly, we define the dimension of the sheath. Our model shows that there exists a limit of the electron density distributions for our conditions of interest at any phase of the voltage. Therefore, we consider as the sheath thickness at any time the distance from the electrode to the electron cloud border where the electron density is one percent of the electron density in the centre of the discharge. Then we average it over the period of the electric field.

In order to calculate the total voltage from the contributions of the sheath and the plasma, it is necessary to consider the differences between the phases of the electric fields in both parts of the discharge and the external voltage applied to the electrodes (see for instance [10]). Let us describe the value of the momentary voltage by:

$$V(x, t) = -\int_0^x E(x, t)\,dx. \tag{4}$$

We denote the voltage drop over the two sheaths by $V_s(t)$ and over the plasma in the centre by $V_p(t)$. The integration in (4) between the electrodes gives then with $V(x = 0) = 0$ the following result:

$$\left.\begin{aligned} V_s(t) &= V(x_L(t)) + [U(t) - V(x_R(t))], \\ V_p(t) &= V(x_R(t)) - V(x_L(t)), \\ U(t) &= U_m \sin \omega t = V_s(t) + V_p(t), \end{aligned}\right\} \tag{5}$$

where x_L and $l - x_R$ are the sheath widths near the left and the right electrodes, respectively, l is the distance between the electrodes, U and U_m are, respectively, the externally applied voltage and its amplitude and ω is the circular frequency of the external voltage.

In considering the external applied voltage as a harmonic function it should be noted that this is in general not the case for the voltage drops over the sheaths and the plasma, respectively. In order to calculate their phase it is necessary to make a Fourier analysis of $V_s(t)$ and $V_p(t)$. From this analysis it is found that the first harmonic for both is dominant under our conditions.[1] The Fourier transformation gives automatically the phase shift between $V_s(t)$ and $V_p(t)$. In Fig. 6 the VIC is shown together with the root-mean-square values for the first harmonics of $V_s(t)$ and $V_p(t)$ and the phase shift ϕ_{sp} between $V_s(t)$ and $V_p(t)$.

The dependence of the plasma voltage on the current has a negative slope. This negative slope is characteristic for a positive glow like a DC discharge. The difference of our case with a DC discharge is only quantitative. The slope of the VIC of the plasma is the RF discharge is slightly less negative than that of a DC discharge. There are two reasons for it. The first one is due to the fact that for increasing current the decreasing field at the centre of the discharge is partially compensated by the increasing field near the edges of plasma region. The second one is the fact that the length of the positive column increases with the current at the expenses of the sheath width.

The calculated results show a maximum for the voltage with increasing current. The VIC of the sheath determines substantially the behaviour of the total VIC. Since for currents higher than that at the maximum $C(C')$ of the VIC, a transition starts from a low current (α) to a high current type of discharge (γ) we focus our attention on the physical reason of this maximum. It can be understood from Fig. 8 where the dependence (at two frequencies 62MHz and 223 MHz) of the sheath width d, and the root-mean-square value of the electric field strength E_{RMS} on the surface of electrode ($x = 0$) are shown as a function of the discharge current. Notice that with the current increase the sheath width decreases and the electric field strength increases. This results in a maximum of the VIC for the sheath. It is very important to point out the strong influence of the current on the sheath width. This fact was never mentioned before. Moreover, it was believed that the sheath width was proportional to $d_0 \approx v_e/\omega$ (v_e is the electron drift velocity in the plasma) and equal to the oscillation amplitude of the electron gas. The data presented here show that our different approach results in a decrease of the sheath width with current. The values of d_0 are shown by the dashed lines in Fig. 8. They are practically horizontal lines with a small positive slope as a result of the small change of $v_e = f(E/N)$ in the plasma. At a low current, up to about 1 A, the practically constant value of the sheath width results to a simple "oscillation" model [10] which is approximately valid. The higher the current the more it deviates from the simple

[1] This is true for $V_s(t)$ as the sum of the voltages near the two electrodes. In general, it is not true for each sheath, separately. The zero (constant voltage) and higher harmonics may then have considerable values

model. In connection with the comprehensive discussions concerning electric parameters (see for instance [1, 9, 10, 13, 14] we mention that in our model charged particles are created in the volume under all conditions. We also considered in our model the secondary emission processes at the electrode surface. However, a secondary-emission coefficient varying from 0.01 to 0.1 really did not influence the present results of our calculations.

3.2 *The influence of frequency on the VIC*

In Fig. 9, the VIC is plotted for three different frequencies of the RF electric field: 62, 125 and 223 MHz. In this figure we show the dependence of the root-mean-square of the voltage over the positive glow, the sheath and the electrodes as a function of the root-mean-square of the current. Several remarkable tendencies can be seen. As the frequency increases the breakdown voltage decreases slightly. The reason is, as the analysis shows, that the losses by electron diffusion are frequency dependent and

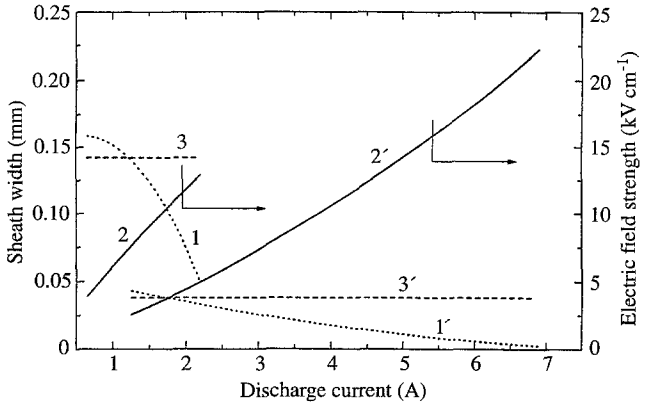

Fig. 8. The dependence of the sheath width and the RMS of the electric field strength near the electrode as a function of the RMS value of the discharge current at a frequency of 62 MHz (1,2,3) and 223 MHz (1′, 2′, 3′), 1 and 1′ are the sheath thickness, 2 and 2′ are the field strength, 3 and 3′ are the current independent sheath thickness

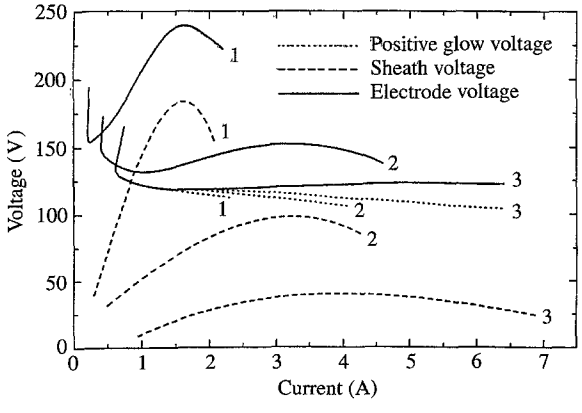

Fig. 9. Discharge VIC's at different frequencies (1) 62 MHz, (2) 125 MHz, (3) 223 MHz

at low input power when the sheaths are not formed yet there is a higher loss at lower frequency. The electrons disappear on the electrodes with the "oscillation" of the electron cloud [10], whereas the electrons are moving from the centre to the edge of the electron cloud by diffusion. At lower frequencies, more electrons reach the electrode because there is more time available and consequently the electron density at the central part decreases. It is quite clear that at different frequencies the breakdown occurs at different values of the current determined by the displacement current I_{dRMS} proportional to ωU_{RMS}, and that the breakdown voltages do not vary much as discussed above.

When the frequency increases the positive VIC slope decreases remarkably and the VIC maximum shifts to a larger current. It results from a change of the voltage space structure. In Fig. 9 as well as in Fig. 6 we have plotted separately the VIC for the positive glow and for the sheath. At, different frequencies the positive glow VIC's nearly coincide whereas the sheath VIC's vary quite strongly.

Let us now consider the VIC without the region of the first negative slope which is the most interesting part of this study (range BCD in Fig. 6). We note that the full VIC at $f = 62$ MHz is determined practically by the sheath VIC and the full VIC at $f = 223$ MHz follows more closely the positive glow VIC with its maximum at a larger current. The physical reason of it can be found in Fig. 8 where we see that at a larger frequency the increase of the electric field outweights the decrease of the sheath thickness with rising current.

3.3 *Influence of frequency on the current stability in the electrical discharge circuit*

From the results presented above we have seen that the RF discharge has a complicated VIC structure with a positive and negative slope. This requires a careful design of the electrical circuit for the power supply.

Despite the clear physical interest for the low current part of the VIC (OAB region in Fig. 6), we will not discuss this item in the present work. For the laser operation it is much more interesting to work in the BCD region with a large input power. The dependence of the input power in the discharge on the conduction current is presented in Fig. 10 for different frequencies. From the Figs. 6 and 9 it is seen that the conduction current and the total current are comparable in the BCD region. In the BC region of the VIC, the discharge is stable with a positive dynamic resistance and the discharge can be simply connected to a voltage supply. However, in the CD region there is a current instability. One possible way for creating a stable self-sustained discharge in this region is to change the discharge structure and its impedance, for example, by transition to a γ type of discharge. However, this possibility is not suitable for homogeneous pumping of a CO_2 laser medium [1].

It is, however, possible to stabilise the total α type current in the region of the negative slope (CD) with, for instance, an additional capacitance in series. The discharge itself will remain homogeneous and not disturbed

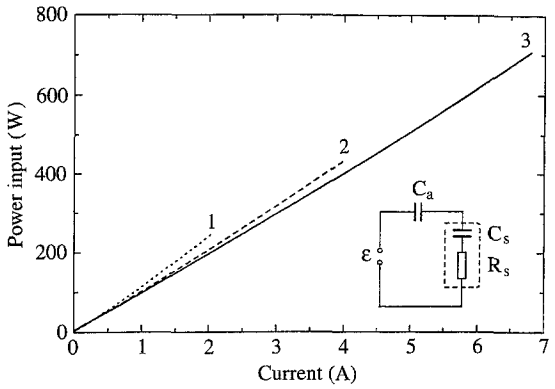

Fig. 10. The dependence of the input power on the conduction current and the equivalent electrical circuit (1) 62 MHz, (2) 125 MHz, (3) 223 MHz

because, in the whole region of the VIC the discharge appears to be stationary and a Townsend's breakdown of the sheath is not present yet.

The equivalent circuit is shown in Fig. 10 where C_s and R_s are the capacitive impedance of the sheath and the active resistance of the positive glow, respectively, and ε is the applied voltage between the electrodes. C_a is the additional capacitance. According to the well-known rules for vector summation (see for instance, [15]), we find for the RMS-value of the applied voltage U_H to the electrodes of the waveguide:

$$U_H(I) = [\varepsilon^2 + I^2 X_a^2 - 2\varepsilon X_a I \cos\varphi]^{1/2}, \tag{6}$$

where I is the RMS-value of the total current $X_a = 1/(\omega C_a)$, $X_s = 1/(\omega C_s)$; $\cos\phi = (X_a + X_s)/Z$; $Z = [(X_a + X_s)^2 + R_s^2]^{1/2}$.

The RMS-value of the voltage $U(I)$ of the VIC is given by:

$$U(I) = I(R_s^2 + X_s^2)^{1/2}. \tag{7}$$

The criterion for a stable stationary current in the electrical circuit with constant voltage of the power supply is [16]:

$$\left|\frac{dU_H(I)}{dI}\right| > \left|\frac{dU(I)}{dI}\right|. \tag{8}$$

Taking the derivative of (6) we obtain:

$$\frac{dU_H}{dI} = \frac{I}{U_H}\left[IX_a^2 - \varepsilon X_a \frac{(X_a + X_s)}{Z} - \frac{\varepsilon X_a I}{Z}\frac{dX_s}{dI} - \frac{\varepsilon X_a I}{Z^2}(X_a + X_s)\frac{dZ}{dI}\right]. \tag{9}$$

After substituting in (8) $Z = \varepsilon/I$, $dZ/dI = -\varepsilon/I^2$ and the condition $U_H(I) = U(I)$ we obtain:

$$\frac{dU_H}{dI} = -\frac{I}{U}\left[2X_a X_s + X_a\frac{dX}{dI} + X_a^2\right]. \tag{10}$$

Condition (8) is now fulfilled when

$$X_a^2 + 2X_a p - q > 0, \tag{11}$$

where

$$p = X_s + \frac{1}{2} I \frac{dX_s}{dI}$$

and $$q = -\frac{U(I)}{I}\frac{dU}{dI} = -(R_s^2 + X_s^2)^{1/2}\frac{dU}{dI},$$

or:

$$X_a > -p + \sqrt{p^2 + q}. \tag{12}$$

In our model we calculated $U(I)$ (see Figs. 6 and 9) and the values of X_s and R_s of the discharge impedance (see [5]).

For the realisation of a discharge on the negative slope of the VIC at a frequency of 62 MHz and an input power of $P_{in} = 200$–250 W it is necessary that $X_a > 40\ \Omega$ and $C_a < 64$ pF. It is interesting to mention Ref. [8], where the limit of the input power was higher when thin quartz plates were placed in between the metal electrodes. These plates form an additional capacitance. In our case, these plates must be $\delta/\varepsilon_d \geq 0.1$ mm according to the above mentioned condition. If we take for quartz a dielectric constant ε_d of about 10 then the plate thickness δ must be more than 1 mm with an electrical strength sufficient to prevent breakdown. This value is close to that in [8] despite the different interpretation.

4 General discussion and conclusions

Finally, we want to discuss how to choose the optimum frequency for the active medium of a CO_2 laser. In Fig. 1, the vertical arrows correspond to the maximum values of the VIC's (points "C" in Figs. 6, 9). For a sealed-off laser with corresponding chemical reactions (solid curves in Fig. 1) and operating at a frequency of 62 MHz the maximum power output can be achieved by a special modification of the power supply circuit. At the frequency of 223 MHz, the maximum power output can be achieved without special provisions. The same situation is true at the frequency of 125 MHz. The higher frequency is preferable because the maximum is at a higher input power as a result of space effects (Figs. 2–5). Frequencies above 223 MHz are not advantageous for two reasons. Firstly, at $f = 223$ MHz the sheath width is much smaller than the discharge thickness and the space factor does not affect very much anymore. Secondly, the higher frequency introduces additional difficulties for distributing the voltage along the laser axis homogeneously [1].

A different situation arises when chemical reactions are suppressed (dotted curves in Fig. 1). This can be realised for example, with a fast gas flow across the laser (a longitudinal flow may not be effective because the time of the flow to pass the cavity is comparable with the CO_2 dissociation time and also because in a narrow channel there will exist a large pressure gradient). In this case a increase of the frequency is even more effective. Our calculation predicts a further increase of the specific output power compared to the existing record values quoted in [4].

Acknowledgements. The present research have been supported by the Netherlands Scientific Organisation (NWO), the Netherlands Technology Foundation (STW), the NATO Collaborative Research Grant (No. 920493) and the Russian Foundation For Basic Research, Grant 96-02-16442.

References

1. D.R. Hall, C.A. Hill: In *Radio Frequency Discharge Excited* CO_2 *Lasers*, Handbook of Molecular Lasers, ed. by P.K. Cheo (Marsel Bekker, New York, 1987)
2. N.I. Lipatov, P.P. Pashinin, A.M. Prokhorov, V.Yu. Yurov: Proc. Institute of General Physics, Moscow, **17**, 53–118 (1980) (in Russian)
3. P.V. Salvo: Industr. Laser Rev. **7**, 9 (1992)
4. M.B. Heeman-Iilieva, Yu.B. Udalov, W.J. Witteman, P.J.M. Peters, K. Hoen and V.N. Ochkin: J. Appl. Phys. **74**, 4786 (1993)
5. B.I. Ilukhin, Yu.B. Udalov, I.V. Kochetov, V.N. Ochkin, M.B. Heeman-Ilieva, P.J.M. Peters and W.J. Witteman: Appl. Phys. B **61** (1995)
6. P.P. Vitruk, N.A. Yatsenkov: Sov. Tech. Phys. Lett. **15**, 163 (1989)
7. D. He, D.R. Hall: IEEE J. Quant. Electron. **QE-20**, 509 (1984)
8. N.A. Yatsenko, Influence of excitation frequency on parameters of RF excited gas laser, Institute of Problem Mechanics, Preprint No. **465** (1990) (in Russian)
9. P. Vidaud, S.M.A. Durrani, D.R. Hall: J. Phys. D: Appl. Phys. **21** (1988)
10. Yu.P. Raizer, *Gas Discharge Physics*, (Springer, Berlin, 1991) p. 450.
11. W.J. Witteman: *The* CO_2 *laser* (Springer, Berlin, 1987)
12. N.A. Yatsenko: Sov. Phys. – Tech. Phys. **33**, 180 (1988)
13. P.P. Vitruk, H.J. Baker, D.R. Hall: J. Phys. D: Appl. Phys. **25**, 1767 (1992)
14. A.V. Nedospasov, V.D. Hait: The basis of physical processes in low temperataure plasma devices, Energoatomizdat, Moscow (1994) p. 224 (in Russian)
15. Yu.P. Raizer, M.N. Schneider: Sov. J. Plasma Phys. **13**, 267 (1987)
16. A.S. Smirnov, L.D. Tsendin: IEEE Trans. on Plasma Sci. **19**, 130 (1991)